A model for the dissociation pulse, afterglow, and laser pulse in the Cu/CuCl double pulse laser

M. J. Kushner[a] amd F. E. C. Culick

California Institute of Technology, Pasadena, California 91125

A model which completely describes the Cu/CuCl double pulse laser is presented. The dissociation discharge pulse and afterglow are simulated and the results are used as initial conditions for an analysis of the pumping discharge pulse and laser pulse. Experimental behavior including the minimum, optimum, and maximum delays between pulses, and the dependence of laser pulse energy on dissociation energy are satisfactorily reproduced. An optimum tube temperature is calculated, and the dependence of laser pulse energy on tube temperature (i.e., CuCl vapor pressure) is explained for the first time.

PACS numbers: 42.55.Hq, 52.80.Hc

I. INTRODUCTION

The Cu/CuCl laser was introduced in 1973 as a way to obtain laser action from copper vapor at temperatures as much as 1000 °C less than those required using elemental copper.[1,2] The technique takes advantage of the high vapor pressure of metallic halides at temperatures below 1000 °C to provide the source of metal atoms.[3-5] In the Cu/CuCl double pulse laser, copper chloride is first dissociated by a discharge pulse producing copper atoms. Laser action is obtained by a second discharge pulse which pumps the copper atoms. As a result of this method, there are three distinct periods which characterize the laser. The first is the dissociation pulse, typically a few hundred nanoseconds long, during which electron impact processes (ionization, dissociation) are important. The second period is the afterglow following the dissociation pulse, typically tens of microseconds long, during which thermal collisional processes are important. The third period is the pumping discharge pulse.

In previous work, we have shown that the interpulse afterglow is important in explaining the laser's performance. Extreme values of electron densities measured during the afterglow have been correlated with extreme values of laser pulse energy produced by the pumping pulse.[6] Perturbing the afterglow by application of a cw glow discharge has been found to increase laser pulse energy by preventing collisional radiative recombination during the afterglow from populating the lower laser level.[7] The rate of current rise of the pumping pulse and the shape of the laser pulse have been found to be functions of the initial conditions provided for the pumping pulse by the interpulse afterglow.[8]

Each of these observations is a result of processes during the afterglow which effect either the ratio of the density of metastable copper (the lower laser level) to ground-state copper or the electron density. The afterglow electron density determines the characteristics of the pumping pulse, mainly the rate of current rise and peak current. The ratio of the density of metastable copper to ground-state copper at the time of the pumping pulse determines whether threshold can be achieved. Because a large fraction of the copper atoms

emerge from the dissociation in the metastable lower laser level (see Fig. 1), there is a minimum time delay between discharge pulses which must pass before enough copper atoms have collisionally relaxed to permit oscillation. Copper atoms are continually reassociating to form the parent molecule, and there is a maximum time delay between discharge pulses beyond which threshold cannot be reached because the copper atom density is too low. Between the minimum delay (microseconds to tens of microseconds) and the maximum delay (tens to hundreds of microseconds) optimum laser energy is obtained after a time interval called the optimum delay. Therefore processes during the afterglow which effect this sequence (dissociation, relaxation, reassociation) can greatly influence laser pulse energy.
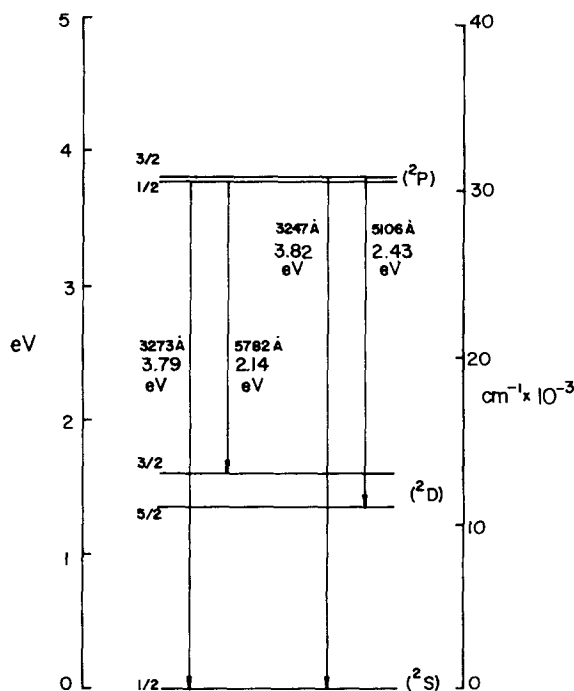

FIG. 1. Partial energy level diagram of neutral copper. The laser transitions at 5782 and 5106 Å terminate on the metastable ^2D level.

---

[a]Present address: Sandia Laboratories, Albuquerque, New Mexico 87185.
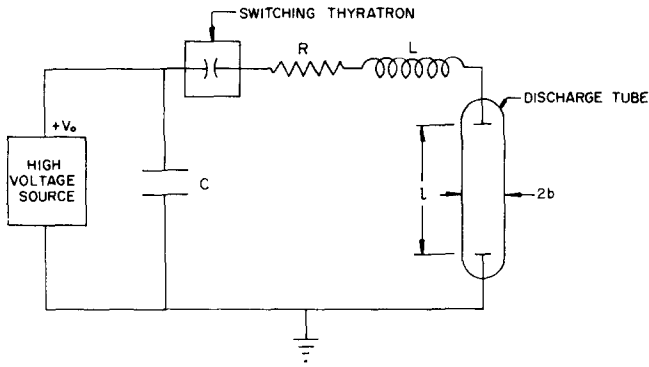
FIG. 2. Circuit used to simulate pulsed power supply. The circuit has lumped resistance R, inductance L, and capacitance C. Typical values are 0.8 Ω, 0.5 μH, and 10 nF.

In this paper, we report the numerical results obtained with a model for the dissociation pulse and interpulse afterglow in a Cu/CuCl double pulse laser. This model provides initial conditions for an analysis of the pumping pulse and laser pulse. We have been able to reproduce successfully much of the experimentally observed behavior, including the dependence of laser energy on time delay and dissociation pulse energy. The existence of an optimum tube temperature (i.e., CuCl vapor pressure) has not previously been adequately explained. Laser pulse energy as a function of tube temperature has been successfully calculated and the reasons for an optimum temperature will be discussed here.

II. A MODEL FOR THE DISSOCIATION PULSE AND AFTERGLOW

The model simulates a discharge through a noble gas/metal halide mixture and the evolution of those species and products during the afterglow. A detailed number and energy balance is kept by simultaneously integrating rate equations for each of the species, as well as the electron temperature, and discharge voltage and current. The method of Runge-Kutta-Gill is used to start the integration and is used to restart the integration whenever the time step is changed. Adams-Moulton predictor-corrector formulas are used for each subsequent time step.[9]

The dissociation pulse is modeled by considering the discharge of a capacitor of capacitance C through the gas mixture. The actual power supply is represented as a simple circuit characterized by a lumped resistance R and inductance L (see Fig. 2). The time rate of change of the voltage across the discharge tube is given by

$$\frac{dV}{dt} = -\frac{I}{C} - R\frac{dI}{dt} - L\frac{d^2I}{dt^2}, \tag{1}$$

where the current I is given by

$$I = n_e A e^2 V / l m_e \nu_c . \tag{2}$$

where A is the cross sectional area of the discharge tube, n_e is the electron density, e is the electronic charge, l is the length of the discharge tube, m_e is the mass of the electron, and ν_c is the electron collision frequency. Integration of the equations begins at the breakdown initiated by the dissociation pulse. To obtain consistent initial conditions the following method

is used. At $t = -t_0 (t_0 \approx 2$ ns) only electrons, helium ions, ground-state helium, and copper chloride are allowed ($n_c = [\text{H}_e^+] \approx 10^9/\text{cm}^3$). The voltage across the discharge tube is assumed to be equal to the capacitor charging voltage V_0. An electron temperature is chosen. Equation (1) and those for the electron temperature [Eq. (20)] and atomic densities (A1–A11) are integrated for t_0 seconds after which dT_e/dt is recorded. This is repeated for a number of initial choices of T_e. The initial conditions at $t = 0$ are then determined by finding the electron temperature at which $dT_e/dt = 0$. This extreme value of the electron temperature is assumed to be the breakdown condition. With these initial conditions, the integration proceeds at $t = 0$.

The following species are included in the model: ions: Cu^+, Cl^+, Cl^-, He^+; metastable species: Cu_m (^2D lower laser level), He_m (2^3S); ground states: Cu, Cl, CuCl, He; and electrons: T_e (Temperature), n_e (density).

The time scale of the afterglow is microseconds to hundreds of microseconds, which is long compared to the radiative lifetime of the atomic excited states. Therefore only the metastable states of helium and copper are included. Only the atomic helium ion is considered. The molecular helium ion He_2^+ is formed by the reaction

$$\text{He}^+ + 2\text{He} \rightarrow \text{He}_2^+ + \text{He} ,$$
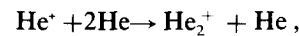
with the rate constant 1.0×10^{-31} cm^6/sec (Ref. 10). It dissociatively recombines by the reaction

$$\text{He}_2^+ + e \rightarrow 2\text{He} ,$$
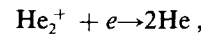
with the rate constant 6×10^{-9} $(T_e/300)^{1/2}$ cm^3/sec.[11] At 5-Torr pressure, milliseconds are required for He_2^+ to become important. This is long compared to times of interest.

Although copper chloride exists primarily as the trimer Cu_3Cl_3 at the temperatures considered here,[12] only the monomer CuCl was included in the model. Most of the rates for reactions with CuCl had to be estimated. More realistic estimates for the monomer could be made by analogy to similar molecules. To have included Cu_3Cl_3 with its many dissociation and reassociation channels would have required too much guesswork, which we regard as unjustified at this time.
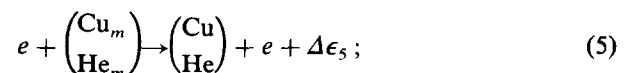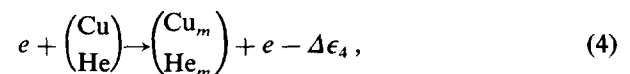
The processes included in the model are listed below. Diffusion processes will be discussed separately.
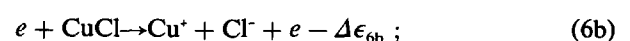
A. Electron impact

(a) Ionization,

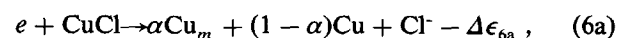$$e + M \rightarrow M^+ + e + e - \Delta\epsilon_3 ; \tag{3}$$
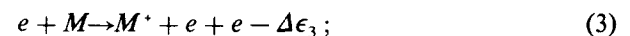
(b) Excitation and supereleastic relaxation of metastable states,

$$e + \binom{\text{Cu}}{\text{He}} \rightarrow \binom{\text{Cu}_m}{\text{He}_m} + e - \Delta\epsilon_4 , \tag{4}$$

$$e + \binom{\text{Cu}_m}{\text{He}_m} \rightarrow \binom{\text{Cu}}{\text{He}} + e + \Delta\epsilon_5 ; \tag{5}$$

(c) Dissociation,

attaching:

$$e + \text{CuCl} \rightarrow \alpha\text{Cu}_m + (1 - \alpha)\text{Cu} + \text{Cl}^- - \Delta\epsilon_{6a} , \tag{6a}$$

$$e + \text{CuCl} \rightarrow \text{Cu}^+ + \text{Cl}^- + e - \Delta\epsilon_{6b} ; \tag{6b}$$

Non-attaching:

$$e + CuCl \rightarrow \alpha Cu_m + (1 - \alpha)Cu + Cl + e - \Delta\epsilon_7 ; \quad (7)$$
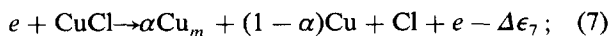
(d) Processes involving Cl^-,

attachment:

$$e + Cl \rightarrow Cl^- , \quad (8)$$

detachment:

$$e + Cl^- \rightarrow Cl + e + e - \Delta\epsilon_9 ; \quad (9)$$
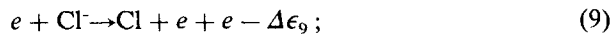
(e) Recombination,

collisional radiative:

$$e + e + M^+ \rightarrow M^*$$
$$+ e + \Delta\epsilon_{10} \rightarrow \delta M_m + (1 - \delta)M + h\nu + e + \epsilon_{10} , \quad (10)$$

radiative:

$$e + M^+ \rightarrow M^* \rightarrow \delta M_m + (1 - \delta)M + h\nu ; \quad (11)$$

Momentum transfer,

$$e + M \rightarrow M + e - \Delta e_{12a} , \quad (12a)$$

$$e + M^+ \rightarrow M^+ + e - \Delta e_{12b} . \quad (12b)$$
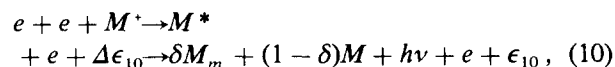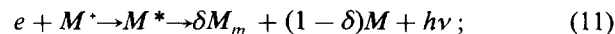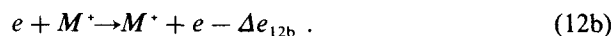
B. Atomic and molecular collisions

(a) Reassociation,

three body:

$$\begin{pmatrix} Cu \\ Cu_m \end{pmatrix} + Cl + M \rightarrow CuCl + M , \quad (13a)$$

neutralizing:

$$Cu^+ + Cl^- \rightarrow CuCl , \quad (13b)$$

detaching:

$$Cu + Cl^- \rightarrow CuCl + e ; \quad (13c)$$
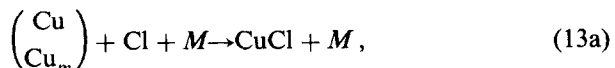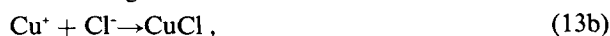
(b) Neutralizing collisions,

$$Cl^- + M^+ \rightarrow Cl + M ; \quad (14)$$

(c) Collisional deactivation,

$$\begin{pmatrix} He_m \\ Cu_m \end{pmatrix} + M \rightarrow \begin{pmatrix} He \\ Cu \end{pmatrix} + M ; \quad (15)$$
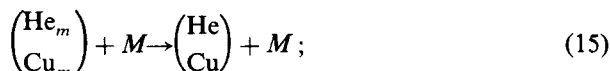
(d) Energy exchange involving metastable or ionized helium,

Penning collisions:

$$He_m + M \rightarrow He + M^+ + e + \Delta\epsilon_{16a} , \quad (16a)$$

$$He_m + He_m \rightarrow He + He^+ + e + \Delta\epsilon_{16b} ; \quad (16b)$$
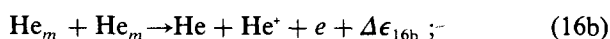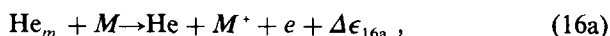
dissociative Penning collisions:

$$He_m + CuCl \rightarrow He + \xi Cu^+ + (1 - \xi)[\alpha Cu_m + (1 - \alpha)Cu]$$
$$+ Cl + \xi e + \Delta\epsilon_{16c} , \quad (16c)$$

charge exchange:

$$He^+ + M \rightarrow He + M^+ ; \quad (17a)$$
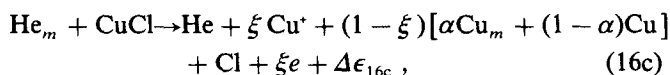
dissociation charge exchange:

$$He^+ + CuCl \rightarrow \eta(Cu^+ + Cl) + (1 - \eta)(Cu + Cl^+) ; \quad (17b)$$
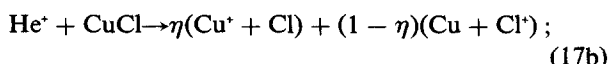
The energy contribution to the electron distribution by process i is $\Delta\epsilon_i$, α is the fraction of copper atoms which emerge from a dissociation of CuCl in the metastable state, and δ is the fraction of ions which recombine into the neutral metastable state. In dissociative Penning reactions, a fraction ξ result in ionizations, and in dissociative charge ex-

change, a fraction η produce copper ions. M is any neutral species, and M^+ is any positive ion. The dominant process for the production of ground-state and metastable copper is nonattaching dissociation of CuCl, process (7). Similarly, the dominant loss mechanism for neutral copper is three-body reassociation of CuCl, process (13a). The production of metastable copper by electron impact of ground-state copper, process (4), is important only when the production due to process (7) is small.

Collisional radiative recombination, process (10), is the dominant form of recombination. Because its electron temperature dependence goes as $T_e^{-9/2}$ (Ref. 13), it becomes important late in the afterglow. The rate of electron-ion recombination by diffusion to the walls is small due to the efficiency of the attaching process (8). The negative chlorine ion becomes the dominant negative charge carrier in times short compared to diffusion times. This slows the rate of recombination at the walls to a value characterized by the gas temperature instead of the electron temperature.

Due to their large threshold energies, excitation and ionization of helium, processes (3) and (4), are important only during the current pulse and early during the afterglow. Once the electron temperature drops and the source of metastable and ionic helium becomes small, Penning collisions, processes (16), and charge exchange collisions, processes (17), rapidly deplete those populations. Superelastic relaxation of metastable helium, process (5), is not an important loss mechanism except at small CuCl vapor pressure, but is important as a source of energetic electrons.

Diffusion losses of minor and charged species are approximated as binary diffusion through the buffer gas. The rate of diffusion is D_i/Λ^2, where D_i is the diffusion coefficient and Λ is the tube diffusion length. For a tube of length l and radius b,

$$1/\Lambda^2 = (\pi/l)^2 + (2.405/b)^2 . \quad (18)$$

For charged particle diffusion[14]

$$D_i^q(T_e) = \tfrac{1}{2}D_i^q(1 + T_e/T_g) , \quad (19)$$

where D_i^q is the ambipolar diffusion constant in thermal equilibrium and T_g is the gas temperature. The boundary conditions at the walls are illustrated in Fig. 3. All charged

$$\mu_x = \frac{\sigma_x^a[x^+]}{\sum_i \sigma_i^a[x_i^+]} \qquad \lambda_x = (1 - \text{fraction of } X^+ \text{ neutralizing } Cl^-)$$
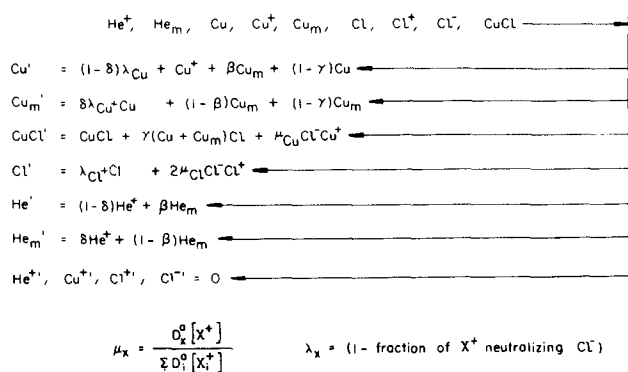
FIG. 3. Charged species and minor neutral species diffuse through the neutal buffer gas to the discharge tube wall where reassociation, relaxation, and recombination occurr. The primed symbols denote the species which return to the plasma from the wall.

particles diffusing to the wall recombine. A fraction $\gamma (\approx 0.5)$ of neutral copper and chlorine reassociate to form CuCl, and all Cl$^-$ + Cu$^+$ neutralizations result in a CuCl molecule. A fraction β (≈ 0.5) of the metastable atoms collisionally relax to form the ground state.

Rate equations for the processes above provide the working equations. The equations are rather involved and are listed in the Appendix.

The electron distribution is assumed to be Maxwellian characterized by the electron temperature T_e. The expression governing the time rate of change in electron temperature is

$$\frac{d}{dt}(\tfrac{3}{2}kT_e)$$

$$= -\sum_i \nu_{e_i}\left(\frac{2m_e}{M_i}\right)\tfrac{3}{2}k\,(T_e - T_g)$$

$$- \sum_i (E_I r_3 + E_m r_4)_i N_i - \frac{D^a}{\Lambda^2}\tfrac{3}{2}kT_e$$

$$+ \sum_i (E_{P_i} - \tfrac{3}{2}kT_e)r_{16}N_i\,\frac{[\mathrm{He}_m]}{n_e} + \sum_i r_{10}n_e N_i^+ \Delta\epsilon_{10}$$

$$+ \sum_i r_5 E_{m_i}N_{m_i} + \frac{e^2 V^2}{l^2 m_e \nu_c}. \tag{20}$$

In Eq. (20), ν_e is the electron elastic collision frequency, r_i is the rate constant for process (i), E_{I_i} is the ionization potential of species i, and E_{m_i} is the excitation energy of the metastable state of species i. The first term on the right-hand side of (20) describes the loss $(2m_e/M)$ of energy suffered by an electron during an elastic collision with an atom or ion. This is the electron "thermalization" term and is particularly important when excitation and ionization rates become small. The second term describes the loss of energy due to inelastic collisions (e.g., excitations, ionizations) and is important during the current pulse and early in the afterglow when the electron temperature is high. The third term represents the energy carried away by electrons diffusing radially to the walls (i.e., diffusion cooling) and is important when the electron temperature is high.

The input of energy to the electrons is represented by the remaining terms of (20). The fourth term is due to Penning ionizations. In a Penning ionization, a "new" electron is injected into the distribution. Its contribution to the average electron energy is proportional to the difference between its initial energy and the average electron energy. The average Penning electron has an initial energy $E_P \approx \tfrac{5}{8}E_{\mathrm{ex}}$, where E_{ex} is the energy excess between the metastable energy and ionization potential of the target.[15] The fifth term of (20) represents recombination heating; the energy carried off by the third-body electron which enables the recombining electron to be captured in an atomic orbital. It is assumed that those atoms not recombining into the metastable state recombine into a state halfway between the metastable state and ionization level. Hence, if a fraction δ recombines into the metastable state,

$$\Delta\epsilon_{10} = \tfrac{1}{2}(1 + \delta)(E_I - E_m). \tag{21}$$

This term makes a relatively minor contribution.

The sixth term is due to superelastic heating; the energy carried off by an electron collisionally relaxing a metastable atom. This term is especially important when the electron temperature is epithermal; that is, when excitation rates are small, but the electron temperature has not yet become thermal. The last term of (20) is due to the energy input from the electric field. It is important only during the current pulse and sets the breakdown electron temperature.
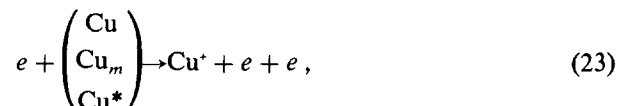
III. THE RATE EQUATION ANALYSIS FOR THE LASER PULSE

With initial conditions provided by the afterglow model, a rate equation analysis is used to simulate the laser pulse and pumping discharge pulse. The electron density, copper ground-state density, copper metastable density, and copper chloride density from the afterglow model are used for initial conditions. The following species are considered in this equation analysis: Cu* (state 3, the upper laser level ^2P), Cu$_m$ (state 2, the lower laser level ^2D), Cu (state 1, the ground state ^2S), CuCl, and $\mathscr{I}$, the cavity intensity. The electron density n_e and electron temperature T_e are specified functions of time.

Due to the short duration of the pumping pulse and laser pulse, processes which proceed at thermal speeds have been ignored. Only electron impact terms and radiative processes are retained. When processes such as Penning ionization with the buffer gas, reassociation and diffusion are included, there is a negligible change in the result. The following processes are considered:
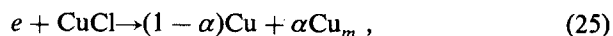
Excitation of the laser levels,

$$e + \mathrm{Cu} \rightarrow \begin{pmatrix} \mathrm{Cu}_m \\ \mathrm{Cu}^* \end{pmatrix} + e, \tag{22}$$

Ionization and electron impact losses,

$$e + \begin{pmatrix} \mathrm{Cu} \\ \mathrm{Cu}_m \\ \mathrm{Cu}^* \end{pmatrix} \rightarrow \mathrm{Cu}^+ + e + e, \tag{23}$$

Superelastic relaxation,

$$e + \begin{pmatrix} \mathrm{Cu}^* \\ \mathrm{Cu}_m \end{pmatrix} \rightarrow \mathrm{Cu} + e, \tag{24}$$

Dissociation,

$$e + \mathrm{CuCl} \rightarrow (1 - \alpha)\mathrm{Cu} + \alpha\mathrm{Cu}_m, \tag{25}$$

Spontaneous emission,

$$\mathrm{Cu}^* \rightarrow \mathrm{Cu}_m + h\nu \tag{26a}$$

$$\mathrm{Cu}^* \rightarrow \mathrm{Cu} + h\nu', \tag{26b}$$

Stimulated emission/absorption,

$$h\nu + \mathrm{Cu}^* \rightarrow \mathrm{Cu}_m + h\nu + h\nu, \tag{27a}$$

$$h\nu + \mathrm{Cu}_m \rightarrow \mathrm{Cu}^*. \tag{27b}$$
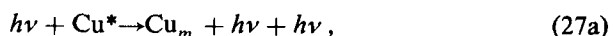
It will be found that dissociation of copper chloride during the pumping pulse, process (25), is one of the more important terms in describing the dependence of laser pulse energy on tube temperature. Process (23), because it causes depletion of the ground state, can be considered a quenching mechanism for the laser pulse since it reduces the pump rate to the upper laser level.

M. J. Kushner and F. E. C. Culick

The electron distribution is assumed to be Maxwellian, with a temperature having a time dependence of $T_e(t) = T_{e0}e^{-t/t'}$, where t' is the full width of the current pulse. This shape closely approximates the experimentally observed[16] and calculated shapes (see Sec. V). The electron density is proportional to the current, and the current pulse is parabolic in shape and 100 ns wide. In order to obtain laser pulse energy as a function of time delay for the initial conditions provided by one dissociation pulse, 25–35 integrations of the laser pulse rate equations are required. A more detailed model, which explicitly solved for the electron temperature, would have been too costly.

The pumping pulse and laser pulse rate equations are

$$\frac{d\,[Cu^*]}{dt} = n_e\{r_{1,3}\,[Cu] - (r^s_{3,1} + r_{3,I})[Cu^*]\}$$
$$- (A_1 + A_2)[Cu^*]$$
$$- ([Cu^*] - (g_3/g_2)[Cu_m])B'\mathscr{I}\,, \qquad (28)$$

$$\frac{d\,[Cu_m]}{dt} = n_e\{r_{1,2}\,[Cu] - (r^s_{2,1} + r_{2,I})[Cu_m]$$

$$+ r_7\,\alpha[CuCl]\} + A_2[Cu^*]$$
$$+ ([Cu^*] - (g_3/g_2)[Cu_m])B'\mathscr{I}\,, \qquad (29)$$

$$\frac{d\,[Cu]}{dt} = n_e(r^s_{2,1}\,[Cu_m] + r^s_{3,1}\,[Cu^*] + (1 - \alpha)r_7[CuCl]$$

$$- (r_{1,3} + r_{1,2} + r_{1,I})[Cu]) + A_1[Cu^*]\,, \qquad (30)$$

$$\frac{d\,[CuCl]}{dt} = - n_e r_7[CuCl]\,, \qquad (31)$$

$$\frac{d\mathscr{I}}{dt} = \mathscr{I}\{B\,([Cu^*] - (g_3/g_2)[Cu_m])$$

$$- c[(1 - \mathscr{R})/l_c - \theta\,]\} + A_2\rho[Cu^*]h\nu c. \qquad (32)$$

A_1 and A_2 are spontaneous emission coefficients, B and B' are stimulated emission coefficients. $\mathscr{R}$ is the output minor reflectivity in an optical cavity of length l_c with parasitic losses θ per unit length. The degeneracy of level i is g_i and the rate constant for excitation between states i and j is r_{ij}. The superscript s denotes a superelastic event. The subscript I denotes the ionization continuum. Processes such as $n_e\,[Cu^*]r_{3,I}$ should be considered a generic electron impact loss.

TABLE I. Reaction rates and cross sections.

(No.)	Process	Rate/cross section	Reference
(3)	$e + M \rightarrow M^* + e + e$	a	20
(4)	$e + Cu \rightarrow Cu_m + e$	a	17
(22)	$e + Cu \rightarrow Cu^* + e$	a	17
(4)	$e + He \rightarrow He_m + e$	a	18
(6a)	$e + CuCl \rightarrow Cu + Cl^-$	b	29[c]
(6b)	$e + CuCl \rightarrow Cu + Cl^* + e$	b	29[c]
(7)	$e + CuCl \rightarrow Cu + Cl + e$	d	20[c]
(8)	$e + Cl \rightarrow Cl^-$	b	28[c]
(9)	$e + Cl^- \rightarrow Cl + e + e$	b	30[c]
(10)	$e + M^* \rightarrow M + h\nu$	$4.2 \times 10^{-12}\left(\dfrac{300}{T_e}\right)^{0.7}$ cm^3/sec	13
(11)	$e + e + M^* \rightarrow M + e + h\nu$	$7.1 \times 10^{-20}\left(\dfrac{300}{T_e}\right)^{4.5}$ cm^6/sec	13,21
(12)	$e + M \rightarrow e + M$	a	32
(13a)	$\binom{Cu}{Cu_m} + Cl + M \rightarrow CuCl + M$	$1 \times 10^{-27}\left(\dfrac{T_g}{300}\right)^{1/2}$ cm^6/sec	26,27[c]
(13b)	$Cu^* + Cl^- \rightarrow CuCl$	$4.0 \times 10^{-10}\left(\dfrac{T_g}{300}\right)^{1/2}$ cm^3/sec	30,31[c]
(13c)	$\binom{Cu}{Cu_m} + Cl^- \rightarrow CuCl + e$	$4.0 \times 10^{-10}\left(\dfrac{T_g}{300}\right)^{1/2}$ cm^3/sec	30,31[c]
(14)	$Cl^- + M^* \rightarrow Cl + M$	$3.0 \times 10^{-7}\left(\dfrac{T_g}{300}\right)^{1/2}$ cm^3/sec	30,31[c]
(15)	$He_m + M \rightarrow He + M$	$6 \times 10^{-15}\left(\dfrac{T_g}{300}\right)^{1/2}$ cm^3/sec	19
(15)	$Cu_m + M \rightarrow Cu + M$	$2 \times 10^{-13}\left(\dfrac{T_g}{300}\right)^{1/2}$ cm^3/sec	26,27[c]
(16a)	$He_m + \binom{Cu}{Cu_m} \rightarrow He + Cu^* + e$	4×10^{-15} cm^2	22[c]
(16a)	$He_m + Cl \rightarrow He + Cl^* + e$	10^{-16} cm^2	22[c]
(16b)	$He_m + He_m \rightarrow He^* + He + e$	$7.1 \times 10^{-8}T_g^{1/6}$ cm^3/sec	25
(16c)	$He_m + CuCl \rightarrow products$	10^{-16} cm^2	22[c]
(17a)	$He^* + \binom{Cu}{Cu_m} \rightarrow He + Cu^*$	2.5×10^{-15} cm^2	23[c]
(17a)	$He^* + Cl \rightarrow He + Cl^*$	4×10^{-15} cm^2	23[c]
(17b)	$He^* + CuCl \rightarrow products$	6×10^{-15} cm^2	24[c]

[a]The reaction rate is obtained by averaging the energy-dependent cross section over a Maxwellian distribution.
[b]For these reactions involving the negative chlorine ion, see the text.
[c]Estimated. See the references for similar reactions or pertinent data.
[d]The electron impact dissociation rate was made the same as an ionization rate, where the dissociation energy [3.8 eV (Ref. 9)] is used instead of the ionization potential.

3024   J. Appl. Phys., Vol. 51, No. 6, June 1980

M. J. Kushner and F. E. C. Culick   3024

The initial electron temperature T_{e0} and peak electron density $n_{e,\max}$ (peak current) are chosen based on the electron density provided by the afterglow model. It has been shown that the rate of current rise and peak current are functions of time delay.[8] It was concluded that the variation in these quantities is partly due to the afterglow electron density present at the time of the pumping pulse. At short time delays, when the afterglow electron density is high, the rate of current rise and peak current are large. As the time delay increases and the electron density decreases, the rate of current rise and peak current decreases, becoming asymptotic to some value associated with long delays. To simulate this behavior, the following scheme is used. If n_e is the density of afterglow electrons at a given time delay, then the peak pumping pulse electron density is

$$n_{e,\max} = n_e + n_{e0},$$

where n_{e0} is the asymptotic value for long time delays. The initial pumping pulse electron temperature is

$$T_{e0} = \begin{cases} \kappa T_{e,\min}, & \kappa < \dfrac{T_{e,\max}}{T_{e,\min}}, \\[2ex] T_{e,\max}, & \kappa > \dfrac{T_{e,\max}}{T_{e,\min}}, \end{cases} \qquad (33)$$

where $\kappa = n_{e,\max}/n_{e0}$. From experimental data,[6,16] we chose $T_{e,\max} = 15.0$ eV, $T_{e,\min} = 5.0$ eV and $n_{e0} = 7.0 \times 10^{13}/\text{cm}^3$.

Only the 5106 Å $^2P_{3/2} \rightarrow {}^2D_{5/2}$ transition is included in the optical model. The first term of (32) is due to stimulated emission (or absorption). By averaging over a Doppler lineshape and gain profile, the stimulated emission coefficient can be written as $(c^4 A_2/32\pi^{5/2}\nu^3)(M_{\text{Cu}}/kT_g)^{1/2}$, where ν is the oscillation frequency, and M_{Cu} is the mass of a copper atom. The second term of (32) describes output coupling and scattering or parasitic losses. The last term of (32) describes the probability ($\rho \approx 10^{-5}$) that spontaneous emission remains in the cavity and forms the basis for stimulated emission.

IV. REACTION RATES AND CROSS SECTIONS

Reaction rates and cross sections are listed in Table I. Electron impact excitation rates are obtained by averaging the energy-dependent cross section over a Maxwellian electron distribution using the current electron temperature. Superelastic cross sections are calculated from the excitation cross sections using the Klein-Rosseland Formula for detailed balancing.[19]

TABLE II. Standard parameters for calculations.

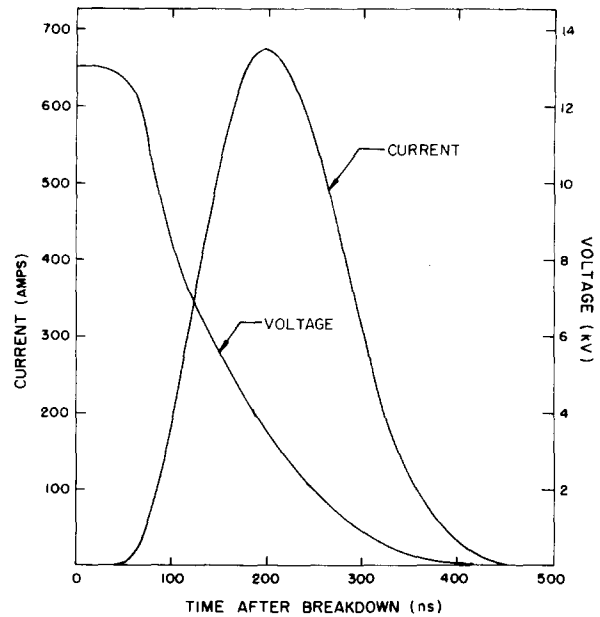|	
Tube temperatures (T_g)	400 °C
Helium pressure	5.0 Torr
Tube length [spacing between electrodes (l)]	65 cm
Tube radius (b)	0.5 cm
Charging potential (V_0)	13.0 kV
Circuit resistance (R)	0.8 Ω
Circuit inductance (C)	0.5 μH
Discharge capacitance (L)	10 nF

FIG. 4. Computed voltage and current for a discharge in 5.0 Torr of helium with the parameters in Table II. ($V_0 = 13$ kV). Peak current is 675 A and FWHM is 165 ns. Typical experimental values are 650–700 A and 150–175 ns.

Electron attachment occurs either by direct attachment to Cl or by dissociative attachment of CuCl. Process (8) takes place at the rate $h\nu_c$, where ν_c is the electron collision frequency with Cl and h is the probability for attachment. ν_c was computed from the elastic collision cross section measured by Cooper and Martin.[28] The attachment probability was estimated to be 5×10^{-4}. The attaching collision [Eq. (6a)] is a resonant process. The threshold energy is $E_d - E_{ea}$, where E_d is the molecular dissociation energy and E_{ea} is the Cl electron affinity. For similar collisions, which produce O⁻ from O_2, NO, CO_2, and CO (Ref. 29), the cross section for process (6a) was estimated to have a peak value of 1.0×10^{-18} cm², a threshold energy of 0.2 eV, and an extent of 4 eV. Process (6b) has a cross section typical of threshold excitation and ionization collisions. The threshold energy is $E_d + E_I - E_{ea}$, where E_I is the copper ionization potential. From similar reactions involving O⁻ (Ref. 29), the form of the cross section was taken to be the same as the ionization cross section having a threshold energy of 7.95 eV and a peak value of 3.0×10^{-19} cm². The electron detachment cross section [Eq. (9) was assumed to be the same as measured by Tiscone and Branscomb[30] for detachment in O⁻.

V. RESULTS AND DISCUSSION

A. A helium afterglow

Standard parameters for the examples which follow are listed in Table II. Voltage and current for a discharge in helium are shown in Fig. 4. Electron temperature and number densities are shown in Fig. 5. The discharge pulse energy is 16.6 mJ/cm³ and has a breakdown electron temperature of 8.6 eV. Peak current is 675 A, and the current pulse has FWHM of 165 ns. These values agree very well with experimental values for similar conditions.

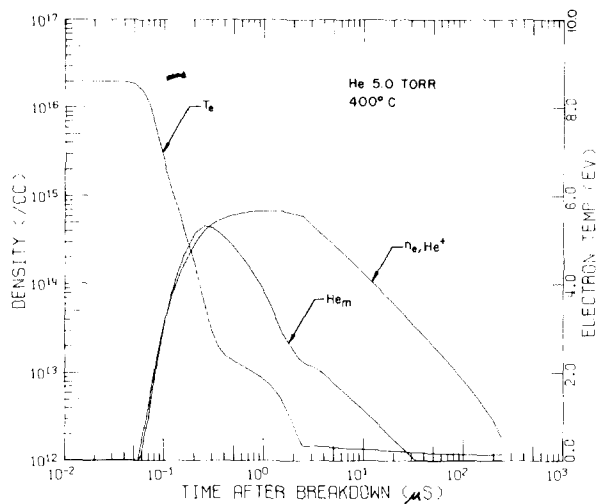M. J. Kushner and F. E. C. Culick   3025

FIG. 5. Density of electrons, helium ions, and helium metastables, and electron temperature for a discharge and afterglow in 5.0 Torr of helium. Note the superelastic electron heating.

Note that the rate at which electrons cool slows down at about 350 ns. This is due to two causes. First, the electron temperature has dropped to a sufficiently low value so that excitation and ionization rates are small. Energy is lost at a slower rate. Second, Penning ionizations and superelastic relaxation of metastable helium produce energetic electrons which heat the distribution. This heating coincides with the decay of metastable helium. (Similar heating has been observed experimentally by Ingraham and Brown.[15]) Note also that the electron density does not drop significantly until the electron temperature becomes asymptotic to the gas temperature. This is indicative of the $T_e^{-9/2}$ temperature dependence of collisional-radiative recombination. Contributions from recombining ions slow the decay of metastable helium at about 3 μs.
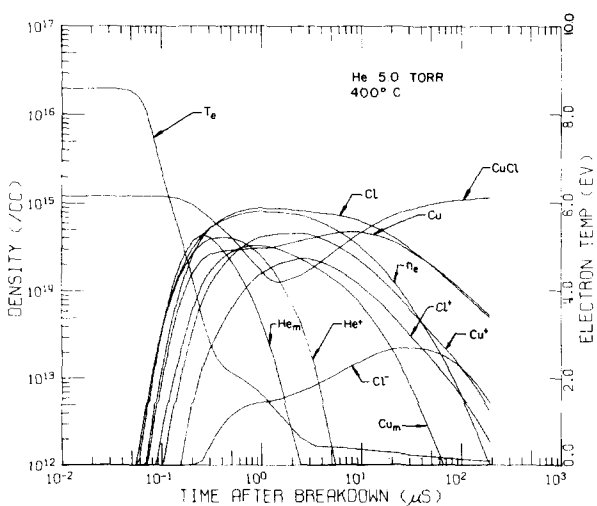

FIG. 6. Discharge and afterglow in 5.0 Torr of helium and CuCl at its vapor pressure for 400 °C. Compare the helium ion and metastable states with the helium discharge. They are quickly depleted due to Penning reactions and charge exchange. Note also that the density of the negative chlorine ion exceeds the electron density after about 65 μs.
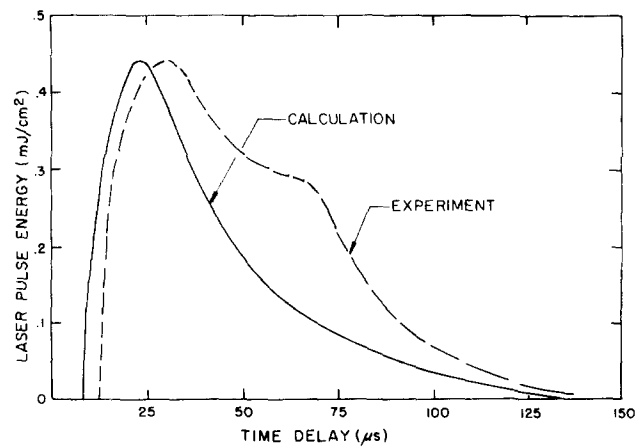

FIG. 7. Laser pulse energy as a function of time delay, calculated using the results of Fig. 6 as initial conditions. The experimental results are for nearly the same discharge conditions. The optimum laser pulse energy was normalized to the calculated value.

B. A He/CuCl afterglow and laser energy as a function of time delay

The results shown in Fig. 6 are obtained using the same discharge conditions as for the helium discharge, but including CuCl at its vapor pressure for 400 °C. The peak current is 625 A, and the current pulse FWHM is 175 ns. The breakdown electron temperature is nearly the same as for pure helium, but the temperature decays more rapidly due to the additional collision partners. Despite the average lower electron temperature, the more easily ionized Cu and Cl cause the peak electron density to be $8.1 \times 10^{14}/cm^3$ compared to the $6.8 \times 10^{14}/cm^3$ in pure helium. Copper becomes the dominant positive ion after a few microseconds into the afterglow due to charge exchange reactions, while Cl⁻ becomes the dominant negative charge carrier by about 65 μs due to electron attaching collisions. (The transition of the dominant positive ion from the noble gas to the metal has been seen experimentally.[33]) Note that the metastable and ionic helium populations are more rapidly depleted than in the pure helium discharge. This is due to Penning and charge exchange collisions. As a result, electron heating from superelastic collisions is less pronounced because the density of metastable helium is smaller.

When densities computed for the He/CuCl discharge are placed in the laser pulse rate equations, laser pulse energy as a function of time delay is obtained (see Fig. 7). Note that we have calculated a minimum, optimum, and maximum delay. The calculation agrees well with experimental results for the same discharge conditions. Experimental laser pulse energy decreases slower after the optimum delay than the computation. This may be the result of using in the analysis a more rapid reassociation of CuCl or pumping rates which decrease more rapidly as a function of time delay than those actually taking place.

The maximum density of ground-state copper is $4.7 \times 10^{14}/cm^3$ and occurs at 7.5 μs, while the optimum delay is about 22 μs when the density of ground-state copper is $3.5 \times 10^{14}/cm^3$. The ratio of copper in the metastable state to ground-state copper at these two times is 0.21 and 0.05. De-
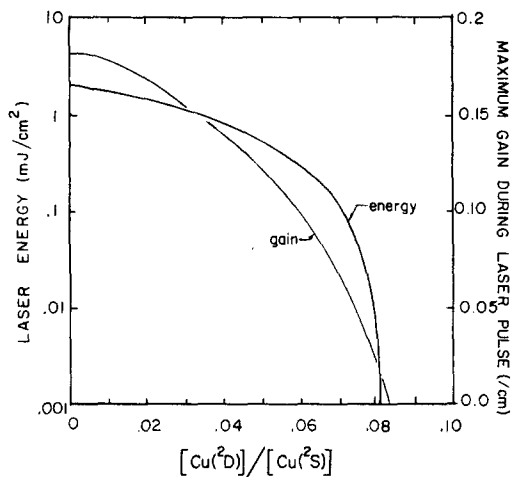
FIG. 8. Laser pulse energy and maximum gain during the laser pulse as a function of the ratio of the density of metastable to ground-state copper ($^2D/^2S$) at the beginning of the pumping pulse. Discharge conditions are otherwise fixed.

spite the larger ground-state density at delays less than optimum, the larger fraction of metastable copper at these delays causes the laser pulse energy to be less than maximum. This is because gain at the start of the pumping pulse will be negative, if metastable atoms are present. For every metastable atom present during the pumping pulse, $1 + g_2/g_3$ ground-state atoms must be excited to the upper level to obtain positive gain. Therefore the density of metastable copper present at the start of the pumping pulse can have a large effect on laser performance. The sensitivity of laser pulse energy to the fraction of metastable copper present at the start of the pumping pulse is shown in Fig. 8. For otherwise fixed conditions, the ratio of metastable to ground-state copper was varied in the rate equations. Note that a small change in the ratio of the metastable to ground-state densities can result in a large change in laser pulse energy and gain.

The rate at which these metastable atoms are formed can be reduced by properly conditioning the dissociation pulse and afterglow. Formation of copper in the metastable state by dissociation of CuCl can be reduced by choosing a long, low-energy dissociation pulse,[34] while the formation of copper in the metastable state by recombining ions can be reduced by preventing the electrons from thermalizing.[7]

C. Optimum laser pulse energy as a function of tube temperature

Since the first report of laser action in metallic halide vapor, the fact that there is an optimum tube temperature (i.e., metal halide vapor pressure) has been a major point of discussion. The increase in laser pulse energy as the tube temperature increases towards optimum is explained by the increase in the CuCl vapor pressure. The decrease in laser pulse energy as the tube temperature increases above optimum has not been satisfactorily explained. Measurements of electron temperatures in a Cu/CuCl laser revealed that the peak electron temperature during the pumping pulse reached a minimum value at the optimum tube temperature.[16] The increase of electron temperature and decrease in

laser pulse energy at temperatures greater than optimum were attributed to Penning ionizations. The idea was that this process would deplete the supply of neutral copper and heat the plasma.

The optimum tube temperature for metallic halide lasers is a function of dissociation pulse and pumping pulse energy, as well as tube geometry and buffer gas pressure. The optimum tube temperature can shift as much as 10 or 20 °C. In particular, as the dissociation pulse energy is increased, the optimum tube temperature increases.[35]

Laser pulse energy (optimized with respect to time delay) as a function of tube temperature, both computed and experimental, are shown in Fig. 9. Note that we have calculated an optimum tube temperature, and that the calculation agrees with the experimental results. The causes for this behavior are discussed below.

At low tube temperatures, the optimum delay nearly coincides with the time at which the peak density of ground-state copper occurs (see Fig. 10). As the tube temperature increases, the time at which the copper density is maximum decreases, and occurs earlier than the optimum delay for the following reasons. Because the reassociation rate of CuCl is proportional to the square of the copper density, as the tube temperature increases, the rate at which copper chloride reassociates increases. Hence the peak ground-state copper density occurs earlier as the tube temperature increases. (This behavior has been seen experimentally.[3]) The collisional relaxation rate of metastable copper increases linearly with density. Because the relative decrease in the density of metastable copper is less than the decreases in the density of ground-state copper due to reassociation, the ratio of the density of metastable to ground-state copper at the optimum delay increases as the tube temperature increases. At tem-
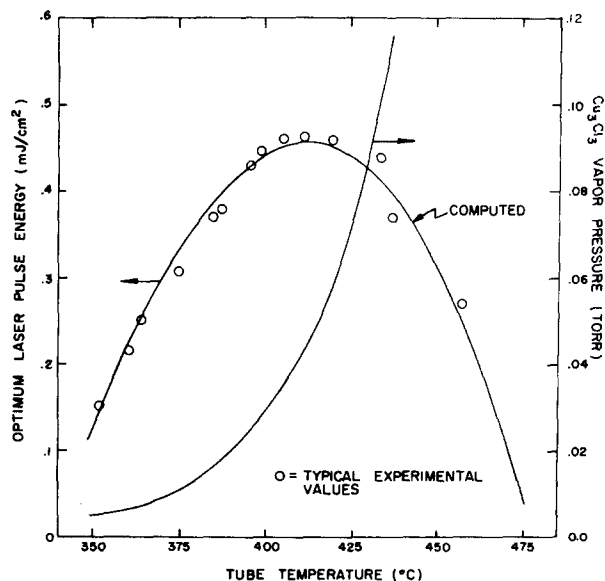

FIG 9. Laser pulse energy optimized with respect to time delay as a function of tube temperature, as computed with the dissociation pulse and afterglow model. The experimental values were normalized to the computed values at the optimum pulse energy. Note the increase in copper chloride vapor pressure as the optimum tube temperature is exceeded.
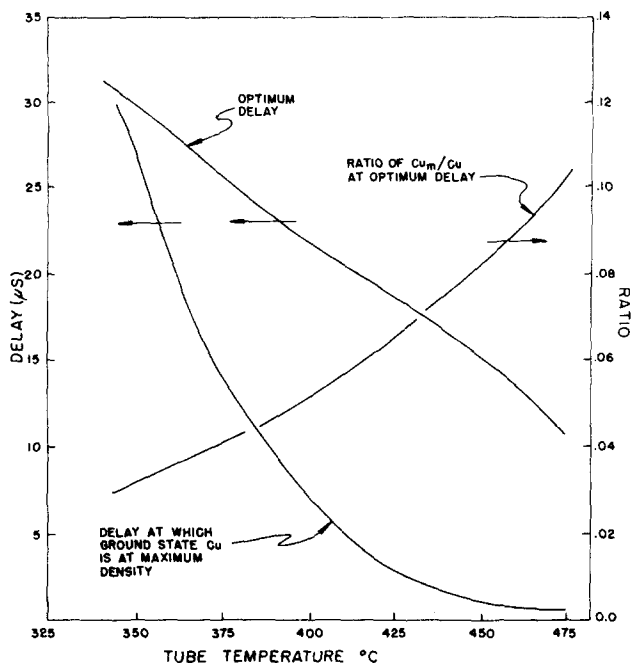
FIG. 10. As the tube temperature increases, the time at which the density of ground-state copper is maximum decreases. The optimum delay also decreases, but at a smaller rate. The ratio of the density of metastable to ground-state copper at the optimum delay increases as the tube temperature increases.

FIG. 12. Computed copper and copper chloride densities as a function of tube temperature. The peak ground-state (^2S) and metastable (^2D) densities of copper are the largest values computed during the dissociation pulse and afterglow. The peak density of ground-state copper, and its value at the optimum delay increase at a smaller rate than the CuCl vapor pressure.

peratures above optimum, the increase in this ratio reduces laser pulse energy.

A second factor contributing to the decrease in laser pulse energy is due to the negative chlorine ion. As the tube temperature increases, the time at which the density of the negative chlorine ion exceeds the electron density decreases [see Fig. 11]. For temperatures above about 430 °C, this change in the dominant negative charge carrier occurs prior to the optimum delay. With increasing tube temperature, the

electron cooling rate increases so that the average electron temperature decreases. Electron detachment rates and ion losses due to diffusion, which are proportional to the electron temperature, also decrease. The net effect is that at a give time delay, as the tube temperature increases, the fraction of negative charge carriers which are electrons decreases.

We have already shown that the pumping rate during the pumping pulse is proportional to the afterglow electron density.[8] Hence the pumping rate at a given time delay decreases, and the optimum pumping rate occurs earlier as the tube temperature increases. (This has been seen experimentally.[8]) At temperatures higher than optimum, the optimum pumping rate occurs when the density of metastable copper is relatively large. This increase in the fraction of copper atoms in the metastable state, when the pumping rate is maximum, decreases the laser pulse energy as the tube temperature is increased.

The third, and perhaps dominant factor in reducing laser pulse energy as the tube temperature and CuCl density increases is due to the CuCl itself. As shown in Fig. 12, the density of copper obtained as a result of the dissociation pulse increases less than the density of CuCl as the tube temperature is increased. At low temperatures, the amount of copper produced by the dissociation pulse is limited by the amount of CuCl present. At high temperatures, the amount of copper obtained is limited by the finite dissociation pulse energy. The ratio of the density of CuCl to ground-state copper, therefore, increases as the tube temperature increases, while the fraction of CuCl dissociated decreases. At sufficiently high temperatures, the CuCl density changes little between the dissociation pulse and pumping pulse. We already know that the fraction of metastable copper obtained in the dissociation of CuCl is so large that oscillation cannot occur unless there is a significant fraction of ground-state copper already present. Hence as the CuCl/Cu density ratio increases with increasing tube temperature, contributions to
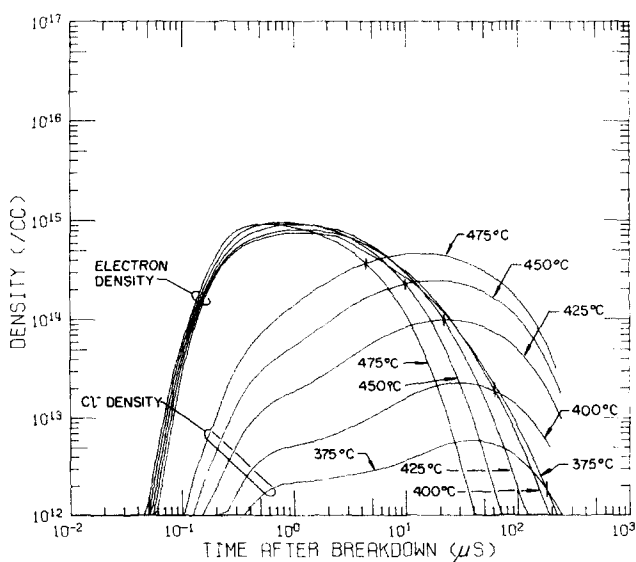

FIG. 11. Electron densities and the density of the negative chlorine ion as a function of tube temperature. The vertical lines denote the time at which the density of the chlorine ion exceeds the electron density. This time decreases as the tube temperature increases.
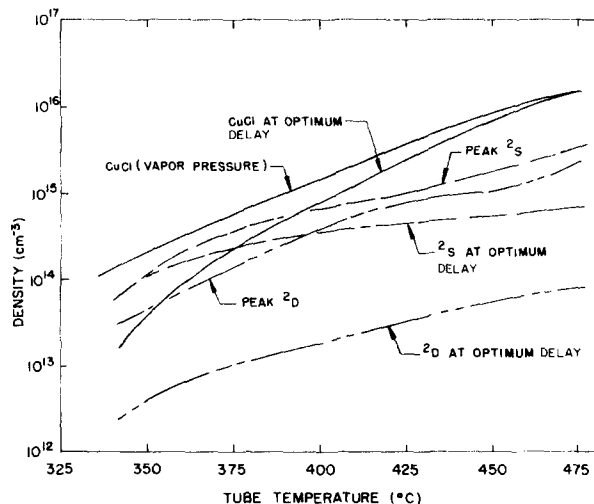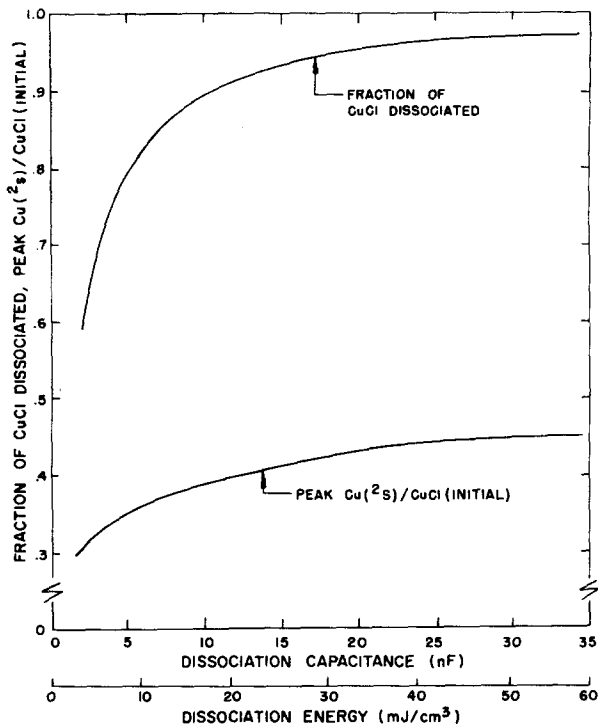
FIG. 13. Fraction of CuCl dissociated by the discharge pulse, and the ratio of the maximum density of ground-state copper during the afterglow to the density of CuCl at the start of the dissociation pulse as a function of dissociation pulse energy. The dissociation pulse energy density is defined as $(\frac{1}{2} CV_0^2)/(\pi b^2 l)$. Note that the peak ground-state copper density increases at a slower rate than the density of dissociated CuCl. Ionizations and excitations deplete the ground state as the discharge energy increases.

the metastable state from CuCl dissociated during the pumping pulse increases. This reduces the laser pulse energy. For sufficiently high tube temperatures, the pumping pulse is actually a second dissociation pulse, which we already know cannot produce a laser pulse.

When the dissociation pulse energy is increased, the ratio of the density of CuCl to ground-state copper decreases at a given temperature (see discussion below). This shifts the optimum density of CuCl to a higher temperature, and accounts for the observed increase in optimum temperature as the dissociation pulse energy is increased.[35]

D. Dissociation pulse energy and the rate of reassociation of CuCl

We have seen that the dependence of laser pulse energy on tube temperature is sensitive to both the degree of dissociation and the rate of reassociation of CuCl. The first is a function of the dissociation pulse energy while the second is a function of the reassociation rate constant. To examine the sensitivity of the laser pulse energy on these quantities, we have carried out some calculations for different values of the dissociation pulse energy and the reassociation rate constant.

For otherwise fixed conditions, variations in the dissociation pulse energy gave the results shown in Fig. 13. Dissociation energy is defined as $\frac{1}{2}CV^2$; the charging voltage was held constant at 13.0 kV. For a given tube temperature, there is a finite amount of copper chloride which can be dissociat-

ed. Therefore, as the dissociation pulse energy is increased, the amount of copper chloride which is dissociated asymptotically approaches the initial copper chloride density. When the dissociation of CuCl approaches 100% during a discharge pulse, the production of ground-state copper decreases. The processes which deplete the ground state (i.e., metastable excitation, ionization) remain. The net affect is that as dissociation pulse energy increases, the increase in the density of ground-state copper is less than the increase in the amount of CuCl which is dissociated.

Maximum laser pulse energy displays the same behavior as does ground-state copper when the dissociation pulse energy is varied. Computed and experimental values for the laser pulse energy are shown in Fig. 14. The calculated behavior agrees well with the experimental results. The increase in laser pulse energy with increasing dissociation pulse energy is due to a higher fraction of copper chloride being dissociated. The saturation of laser pulse energy as the dissociation pulse energy is increased is due to the finite amount of CuCl available for dissociation and to the depletion of ground-state copper from excitations and ionizations.

Laser pulse energy at the optimum delay and the characteristic delays as a function of the reassociation rate of CuCl are shown in Fig. 15. For a small change in the reassociation rate, a large change in laser pulse energy is obtained. The influence of the rate of reassociation of CuCl on laser pulse energy is large, primarily for two reasons. The obvious reason is that for otherwise fixed conditions, the larger the reassociation rate, the smaller the density of ground-state copper at a given time delay. The second less obvious reason is that for otherwise fixed conditions, the larger the reassociation rate, the larger the density of CuCl at a given time delay. The amount of CuCl dissociated during the pumping
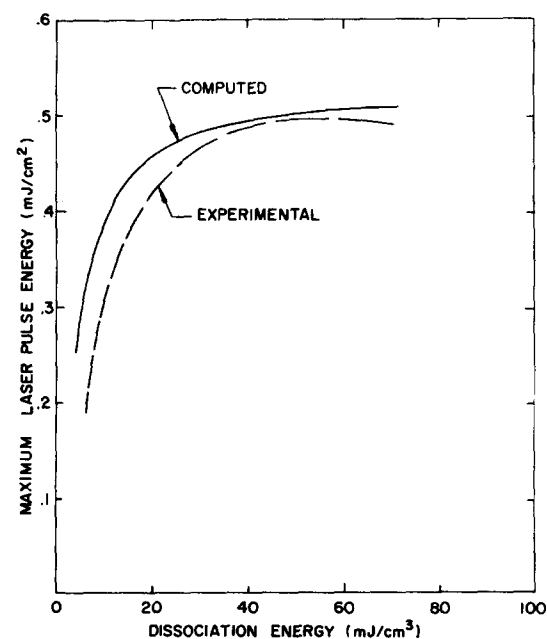

FIG. 14. Laser pulse energy at the optimum delay as a function of dissociation pulse energy density. The experimental values (Ref. 36) were normalized to the computed values at the maximum laser pulse energy.
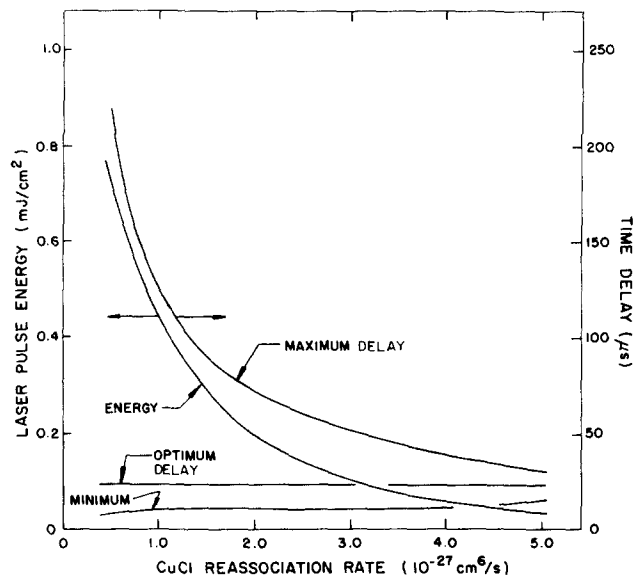
FIG. 15. Laser pulse energy at the optimum delay, and the minimum, optimum, and maximum time delays as a function of the rate of reassociation of CuCl. Optimum laser pulse energy and the maximum delay decrease rapidly as the reassociation rate increases. This is partly due to the increase in CuCl dissociated during the pumping pulse which populates the lower laser level.

pulse and making contributions to the metastable state is also larger. Hence a large reassociation rate not only depletes the ground-state copper reservoir during the afterglow, but also increases contributions to the metastable state during the pumping pulse.

Gabay et al.[37] found that for optimum conditions, the laser pulse energy with CuBr as a source was larger than for CuCl, and CuCl yielded larger laser pulse energy than CuI. The reassociation rate is intrinsic to the particular molecule and is not a sensitive function of other conditions. In view of the sensitivity of laser pulse energy on the reassociation rate, it is plausible that the results of Gabay et al. can in part be explained by differing rates of reassociation of the three copper halides.

VI. SUMMARY

A dissociation pulse and afterglow model for the Cu/CuCl double pulse laser has been described. The results obtained by solving rate equations for the pumping pulse and laser pulse provide laser pulse energy as a function of time delay. We have successfully reproduced experimentally observed behavior including the minimum, optimum, and maximum time delays; and the maximum laser pulse energy as a function of dissociation pulse energy and tube temperature.

Based on the results discussed here, we believe that the decrease in laser pulse energy observed in the Cu/CuCl double pulse laser as the tube temperature exceeds the optimum value is due to the following causes: (a) As the copper chloride density increases, the reassociation rate increases with the square of the density, while the metastable copper relaxation rate increases linearly with density. Hence the ratio of the density of ground-state copper to metastable state copper decreases as the temperatures increase. (b) As the tube temperature increases, the fraction of negative charge carried by chlorine ions at any given delay increases, while the fraction carried by electrons decreases. This reduces pumping rates during the pumping pulse, and causes the maximum pumping rate to occur earlier when the fraciton of metastable copper is larger. (c) As the vapor pressure of copper chloride increases, the fraction of CuCl dissociated decreases, and the ratio CuCl/Cu increases. Contributions to the metastable state from dissociated copper chloride during the pumping pulse reduces laser pulse energy.

ACKNOWLEDGMENTS

APPENDIX

We present in this appendix the rate equations used in the dissociation pulse and afterglow model. The equation for the electron temperature can be found in Sec. II, while the equations for the pumping pulse and laser pulse are listed in Sec. III. The factor f_i accounts for differing rates of diffusion.

$$\frac{d[Cu]}{dt} = \frac{(1-\delta)}{A^2} D^a_{Cu^+}[Cu^+]\left(1 - \frac{[Cu^-]}{n_e + [Cu^-]}\right) + \frac{\beta D_{Cu_m}}{A^2}[Cu_m] - \frac{\gamma D_{Cu}}{A^2}[Cu]f_1 - [Cu]n_e(r_3+r_4) + [Cu_m]n_e r_5$$

$$+ (1-\alpha)[CuCl]n_e(r_{6a}+r_7) + (1-\delta)[Cu^+]n_e(n_e r_{10}+r_{11}) - [Cu][Cl][M]r_{13a} - [Cu][Cl^-]r_{13c}$$

$$+ (1-\delta)[Cu^+][Cl^-]r_{14} + [Cu_m][M]r_{15} - [Cu][He_m]r_{16a} + (1-\alpha)(1-\xi)[He_m][CuCl]r_{16b}$$

$$- [Cu][He^+]r_{17a} + (1-\alpha)(1-\eta)[He^+][CuCl]r_{17b}.$$ (A1)

$$\frac{d[Cu_m]}{dt} = \frac{\delta D^a_{Cu^+}}{A^2}[Cu^+]\left(1 - \frac{[Cl^-]}{n_e + [Cl^-]}\right) + \frac{\beta D_{Cu_m}}{A^2}[Cu_m] - \frac{\gamma D_{Cu_m}}{A^2}[Cu_m]f_1 - [Cu_m]n_e r_3 - [Cu_m]n_e r_5$$

$$+ \alpha[CuCl]n_e[r_{6a}+r_7] + \delta[Cu^+]n_e(n_e r_{10}+r_{11}) - [Cu_m][Cl][M]r_{13a} - [Cu_m][Cl^-]r_{13c}$$

$$+ \delta[Cu^+][Cl^-]r_{14} - [Cu_m][M]r_{15} - [Cu_m][He_m]r_{16a} + \alpha(1-\xi)[He_m][CuCl]r_{16b}$$

$$- [Cu_m][He^+]r_{17a} + \alpha(1-\eta)[He^+][CuCl]r_{17b}.$$ (A2)

$$\frac{d\,[\mathrm{Cu}^{\cdot}]}{dt} = -\frac{D^{a}_{\mathrm{Cu}^{\cdot}}}{\Lambda^{2}}\,[\mathrm{Cu}^{\cdot}] + n_{e}r_{3}[\mathrm{Cu}] + n_{e}r_{3}[\mathrm{Cu}_{m}] + n_{e}r_{6b}\,[\mathrm{CuCl}] - [\mathrm{Cu}^{\cdot}]n_{e}(n_{e}r_{10} + r_{11})$$
$$- [\mathrm{Cu}^{\cdot}][\mathrm{Cl}^{-}](r_{13b} + r_{14}) + [\mathrm{He}_{m}]r_{16a}([\mathrm{Cu}] + [\mathrm{Cu}_{m}]) + \xi\,[\mathrm{He}_{m}][\mathrm{CuCl}]r_{16b}$$
$$+ [\mathrm{He}^{+}]r_{17a}([\mathrm{Cu}] + [\mathrm{Cu}_{m}]) + \eta[\mathrm{He}^{+}][\mathrm{CuCl}]r_{17b}\,. \tag{A3}$$

$$\frac{d\,[\mathrm{Cl}]}{dt} = \frac{D^{a}_{\mathrm{Cl}^{\cdot}}\,[\mathrm{Cl}^{\cdot}]}{\Lambda^{2}} + \frac{D^{a}_{\mathrm{Cl}^{\cdot}}}{\Lambda^{2}}\,[\mathrm{Cl}^{\cdot}]f_{3}\frac{D^{a}_{\mathrm{Cl}^{\cdot}}\,[\mathrm{Cl}^{\cdot}] + D^{a}_{\mathrm{He}^{\cdot}}\,[\mathrm{He}^{\cdot}]}{D^{a}_{\mathrm{Cl}^{\cdot}}\,[\mathrm{Cl}^{\cdot}] + D^{a}_{\mathrm{Cu}^{\cdot}}\,[\mathrm{Cu}^{\cdot}] + D^{a}_{\mathrm{He}^{\cdot}}\,[\mathrm{He}^{\cdot}]}$$
$$- \frac{\gamma D_{\mathrm{Cl}}}{\Lambda^{2}}\,[\mathrm{Cl}]f_{2} - n_{e}r_{3}[\mathrm{Cl}] + n_{e}r_{7}[\mathrm{CuCl}] - n_{e}r_{8}[\mathrm{Cl}] + n_{e}r_{9}[\mathrm{Cl}^{-}] + [\mathrm{Cl}^{\cdot}]n_{e}(n_{e}r_{10} + r_{11})$$
$$- ([\mathrm{Cu}] + [\mathrm{Cu}_{m}])[\mathrm{Cl}][M]r_{13a} + 2[\mathrm{Cl}^{\cdot}][\mathrm{Cl}^{\cdot}]r_{14} + [\mathrm{Cl}^{-}]([\mathrm{Cu}^{\cdot}] + [\mathrm{He}^{\cdot}])r_{14} - [\mathrm{He}_{m}][\mathrm{Cl}]r_{16a}$$
$$+ [\mathrm{He}_{m}][\mathrm{CuCl}]r_{16b} - [\mathrm{He}^{\cdot}][\mathrm{Cl}]r_{17a} + \eta[\mathrm{He}^{\cdot}][\mathrm{CuCl}]r_{17b}\,. \tag{A4}$$

$$\frac{d\,[\mathrm{Cl}^{\cdot}]}{dt} = -\frac{D^{a}_{\mathrm{Cl}^{\cdot}}\,[\mathrm{Cl}^{\cdot}]}{\Lambda^{2}} + n_{e}r_{3}[\mathrm{Cl}] - n_{e}\,[\mathrm{Cl}^{\cdot}](n_{e}r_{10} + r_{11}) - [\mathrm{Cl}^{\cdot}][\mathrm{Cl}^{-}]r_{14} + [\mathrm{He}_{m}][\mathrm{Cl}]r_{16a}$$
$$+ [\mathrm{He}^{\cdot}][\mathrm{Cl}]r_{17a} + (1 - \eta)[\mathrm{He}^{\cdot}][\mathrm{CuCl}]r_{17b}\,. \tag{(A5)}$$

$$\frac{d\,[\mathrm{Cl}^{-}]}{dt} = -\frac{D^{a}_{\mathrm{Cl}}\,[\mathrm{Cl}^{-}]}{\Lambda^{2}} + n_{e}\,[\mathrm{CuCl}](r_{6a} + r_{6b}) + n_{e}\,[\mathrm{Cl}]r_{8} - n_{e}\,[\mathrm{Cl}^{-}]r_{9}$$
$$- [\mathrm{Cu}^{\cdot}][\mathrm{Cl}^{-}]r_{13b} - [\mathrm{Cu}][\mathrm{Cl}^{-}]r_{13c} - [\mathrm{Cl}^{-}][M^{\cdot}]r_{14}\,. \tag{A6}$$

$$\frac{d\,[\mathrm{CuCl}]}{dt} = -\frac{d\,[\mathrm{Cu}]}{dt} - \frac{d\,[\mathrm{Cu}_{m}]}{dt} - \frac{d\,[\mathrm{Cu}^{\cdot}]}{dt} = -\frac{d\,[\mathrm{Cl}]}{dt} - \frac{d\,[\mathrm{Cl}^{\cdot}]}{dt} - \frac{d\,[\mathrm{Cl}^{-}]}{dt}$$
$$= \gamma f_{1}\frac{(D_{\mathrm{Cu}_{m}}\,[\mathrm{Cu}_{m}] + D_{\mathrm{Cu}}\,[\mathrm{Cu}])}{\Lambda^{2}} + \frac{D^{a}_{\mathrm{Cu}^{\cdot}}}{\Lambda^{2}}\,[\mathrm{Cu}^{\cdot}]\left(\frac{[\mathrm{Cl}^{-}]}{n_{e} + [\mathrm{Cl}^{-}]}\right)$$
$$- n_{e}\,[\mathrm{CuCl}](r_{6a} + r_{6b} + r_{7}) + ([\mathrm{Cu}] + [\mathrm{Cu}_{m}])[\mathrm{Cl}][M]r_{13a} + [\mathrm{Cu}^{\cdot}][\mathrm{Cl}^{-}]r_{13b}$$
$$+ ([\mathrm{Cu}] + [\mathrm{Cu}_{m}])[\mathrm{Cl}^{-}]r_{13c} - [\mathrm{He}_{m}][\mathrm{CuCl}]r_{16b} - [\mathrm{He}^{\cdot}][\mathrm{CuCl}]r_{17b}\,. \tag{A7}$$

$$\frac{d\,[\mathrm{He}_{m}]}{dt} = -\frac{\beta D_{\mathrm{He}_{m}}}{\Lambda^{2}}\,[\mathrm{He}_{m}] + \frac{\delta D^{a}_{\mathrm{He}^{\cdot}}}{\Lambda^{2}}\,[\mathrm{He}^{\cdot}] - n_{e}\,[\mathrm{He}_{m}]r_{3} + n_{e}\,[\mathrm{He}]r_{4}$$
$$- n_{e}\,[\mathrm{He}_{m}]r_{5} + \delta[\mathrm{He}^{\cdot}]n_{e}(n_{e}r_{10} + r_{11}) + \delta[\mathrm{He}^{\cdot}][\mathrm{Cl}^{-}]r_{14} - [\mathrm{He}_{m}][M]r_{15}$$
$$- [\mathrm{He}_{m}]([\mathrm{Cu}] + [\mathrm{Cu}_{m}])r_{16a} - [\mathrm{He}_{m}][\mathrm{Cl}]r_{16a} - [\mathrm{He}_{m}][\mathrm{CuCl}]r_{16b} - 2[\mathrm{He}_{m}][\mathrm{He}_{m}]r_{16a}\,. \tag{A8}$$

$$\frac{d\,[\mathrm{He}^{\cdot}]}{dt} = -\frac{D^{a}_{\mathrm{He}^{\cdot}}}{\Lambda^{2}}\,[\mathrm{He}^{\cdot}] + n_{e}\,[\mathrm{He}]r_{4} + n_{e}\,[\mathrm{He}_{m}]r_{4} - [\mathrm{He}^{\cdot}]n_{e}(n_{e}r_{10} + r_{11}) - [\mathrm{He}^{\cdot}][\mathrm{Cl}^{-}]r_{14} - [\mathrm{He}^{\cdot}]([\mathrm{Cu}]$$
$$+ [\mathrm{Cu}_{m}])r_{17a} - [\mathrm{He}^{\cdot}][\mathrm{Cl}]r_{17a} - [\mathrm{He}^{\cdot}][\mathrm{CuCl}]r_{17b}\,. \tag{A9}$$

$$\frac{d\,[\mathrm{He}]}{dt} = -\frac{d\,[\mathrm{He}_{m}]}{dt} - \frac{d\,[\mathrm{He}^{\cdot}]}{dt}$$
$$= \frac{\beta D_{\mathrm{He}_{m}}}{\Lambda^{2}}[\mathrm{He}_{m}] + (1 - \delta)\frac{D^{a}_{\mathrm{He}^{\cdot}}}{\Lambda^{2}}\,[\mathrm{He}^{\cdot}] - n_{e}\,[\mathrm{He}](r_{3} + r_{4}) + n_{e}\,[\mathrm{He}_{m}]r_{5}$$
$$+ (1 - \delta)[\mathrm{He}^{\cdot}]n_{e}(n_{e}r_{10} + r_{11}) + (1 - \delta)[\mathrm{He}^{\cdot}][\mathrm{Cl}^{-}]r_{14} + [\mathrm{He}_{m}][M]r_{15}$$
$$+ [\mathrm{He}_{m}]([\mathrm{Cu}] + [\mathrm{Cu}_{m}])r_{16a} + [\mathrm{He}_{m}][\mathrm{Cl}]r_{16a} + [\mathrm{He}_{m}][\mathrm{CuCl}]r_{16b} + 2[\mathrm{He}_{m}][\mathrm{He}_{m}]r_{16c}$$
$$+ [\mathrm{He}^{\cdot}]([\mathrm{Cu}] + [\mathrm{Cu}_{m}])r_{17a} + [\mathrm{He}^{\cdot}][\mathrm{Cl}]r_{17a} + [\mathrm{He}^{\cdot}][\mathrm{CuCl}]r_{17b}\,. \tag{A10}$$

$$\frac{dn_{e}}{dt} = \frac{d\,[\mathrm{Cu}^{\cdot}]}{dt} + \frac{d\,[\mathrm{Cl}^{\cdot}]}{dt} + \frac{d\,[\mathrm{He}^{\cdot}]}{dt} - \frac{d\,[\mathrm{Cl}^{-}]}{dt}\,. \tag{A11}$$

[1]C.J. Chen, N.M. Nerheim, and G.R. Russell, Appl. Phys. Lett. **23**, 514 (1973).

[2]C.S. Liu, E.W. Sucov, and L.A. Weaver, Appl. Phys. Lett. **23**, 92 (1973).

[3]J. Tennenbaum, I. Smilanski, S. Gabay, G. Erez, and L.A. Levin, J. Appl. Phys. **49**, 2662 (1978).

[4]C.J. Chen. Appl. Phys. Lett **24**, 499 (1974).

[5]M.S. Chow and T.A. Cool, J. Appl. Phys. **47**, 1055 (1976).

[6]M.J.Kushner and F.E.C. Culick, Appl. Phys. Lett. **33**, 728 (1978).

[7]M.J. Kushner and F.E.C. Culick, J. Quantum Electron **15**, 835 (1979).

[8]M.J. Kushner and F.E.C. Culick, J. Quan. Electron. (to be published).

[9]K. Matsumoto, Computer Code, California Institute of Technology, 1976.

[10]J.M. Berlande, R. Cheret, A. Deloche, A. Gonfalone, and C. Manus, Phys. Rev. A **1**, 887 (1970).

[11]J.N. Bardsley and M.A. Biondi, Adv. At. Mol. Phys. **6**, 1 (1970).

[12]L. Brewer and N.L. Lofgren, J. Am. Chem. Soc. **72**, 3038 (1950).

[13]M.A. Biondi, in *Principles of Laser Plasmas*, edited by George Bekefi (Wiley Interscience, New York, 1976), pp. 125–158.

[14]M.A. Biondi, Phys. Rev. **93**, 1136 (1954).

[15]J.C. Ingraham and S.C. Brown, Phys. Rev. **138**, A1015 (1965).

[16]E. Sovero, C.J. Chen, and F.E.C. Culick, J. Appl. Phys. **47**, 4538 (1976); N.M. Nerheim and C.J. Chen, DARPA #2756, Jet Propulsion Laboratory, 1976.

[17]S. Trajmar, W. Williams, and S.K. Srivastava, J. Phys. B **10**, 3323 (1977).

[18]W.L. Borst, Phys. Rev. A **9**, 1195 (1974).

[19]A.C.G. Mitchell and M.W. Zemansky, *Resonance Radiation and Excited Atoms*, (Cambridge University, New York, 1971).

[20]C. Deutsch, J. Appl. Phys. **44**, 1142 (1973).

3031   J. Appl. Phys., Vol. 51, No. 6, June 1980

M. J. Kushner and F. E. C. Culick   3031

[21]D.R. Bates and A. Dalgarno, in *Atomic and Molecular Processes*, edited by D.R. Bates (Academic, New York, 1962).

[22]M.A. Biondi, Phys. Rev. **88**, 660 (1952); M.A. Biondi, Phys. Rev. **90**, 730 (1953); T.B. Cook, W.P. West, F.B. Dunning, R.D. Rundel, and R.F. Stebbings, J. Geophys. Res. **79**, 678 (1974); L.A. Cross and M. Cem Gokay, J. Appl. Phys. **49**, 2639 (1978); H. Kano, T. Shay, and G.J. Collins, Appl. Phys. Lett. **27**, 610 (1975); E.W. McDaniel, *Collision Phenomena in Ionized Gases*, (Wiley, New York, 1964); J.T, Mosley, J.R. Peterson, D.C. Lorents, and M. Hollstein, Phys. Rev. A **6**, 1025 (1972); L.A. Riseberg, W.F. Parks, and L.D. Schearer, Phys. Rev. A **8**, 1962 (1973); A.L. Schmeltekopf and F.C. Fehsenfeld, J. Chem. Phys. **53**, 3173 (1970); W.P. Sholette and E.E. Muscheitz, Jr., J. Chem. Phys. **36**, 3368 (1962).

[23]G.J. Collins, R.C. Jensen, and W.R. Bennet, Appl. Phys. Lett. **19**, 125 (1971). E.L. Duman and B.M. Smirnov, High Temp. **12**, 431 (1974); D.J. Dyson, Nature **207**, 361 (1965); H. Kano, T. Shay, and G.J. Collins, Appl. Phys. Lett. **27**, 610 (1975); T. Shay, H. Kano, and G.J. Collins, Appl. Phys. Lett. **26**, 531 (1975); R. Shuker, Y. Binur, and A. Szohe, Phys. Rev. A **12**, 515 (1975).

[24]F.C. Fehsenfeld, A.L. Schmeltekopf, P.D. Goldan, H.I. Schiff, and E.E. Ferguson, J. Chem. Phys. **44**, 4087 (1966); L. Friedman and T.F. Moran, J. Chem. Phys. **42**, 2624 (1965).

[25]I.Ya. Fugol, O.N. Grigorashchenko, and D.A. Myshicis, Sov. Phys. JETP **33**, 227 (1971).

[26]N.M. Nerheim, J. Appl. Phys. **48**, 3244 (1977).

[27]C.S. Liu, D.W. Feldman, J.L. Pack, and L.A. Weaver, Westinghouse R & D Center, Pittsburgh, Pennsylvania, December, 1977 (unpublished).

[28]J.W. Cooper and J.B. Martin, Phys. Rev. **126**, 1482 (1962).

[29]J.D. Craggs and B.A. Tozer, Proc. Roy Soc. (London) A **247**, 337 (1958); H.D. Hagstrun and J.T. Tate, Phys. Rev. **59**, 354 (1941); E.W. McDaniel, *Collision Phenomena In Ionized Gases* (Wiley, New York, 1964); A.N. Prasad and J.D. Craggs, in *Atomic and Molecular Processes*, edited by D.R. Bates (Academic, New York, 1962); G.J. Shulz, Phys. Rev. **128**, 178 (1962).

[30]G.C. Tiscone and L.M. Branscomb, Phys. Rev. **170**, 169 (1968).

[31]E.E. Ferguson, F.C. Fehsenfeld, and A.L. Schmeltekopf, Adv. Chem. Ser. **80**, 83 (1969); E.W. McDaniel, V. Cermak, A. Dalgarno, E.E. Ferguson, and L. Friedman, *Ion Molecule Reactions* (Wiley-Interscience, New York, 1970).

[32]L.J. Kieffer, Joint Institute for Laboratory Astrophysics Report No. COM-74-11661.

[33]A.G. Gridnev, T.M. Gorbunova, V.F. Elaev, G.S. Evtushenko, N.V. Osipova, and A.N. Soldatov, Sov. J. Quantum Electron. **8**, 656 (1978)

[34]M. Brandt and J. Piper, presented at SPIE Lasers 78, Orlando, Florida, 1978 (unpublished).

[35]R.K. Bartman (private communication).

[36]N.M. Nerheim, J. Appl. Phys. **48**, 1186 (1977).

[37]S. Gabay, I. Smilanski, L.A. Levin and G. Erez, IEEE J. Quantum Electron. **QE-13**, 364 (1977).